THE JOURNAL OF PHYSICAL CHEMISTRY C

Subscriber access provided by Northern Illinois University

Article

Hydrogen Spillover Enhanced Hydriding Kinetics of Palladium-Doped Lithium Nitride to Lithium Imide

Chikai Lin, Tao Xu, Jiamei Yu, Qingfeng Ge, and Zhili Xiao

J. Phys. Chem. C, **2009**, 113 (19), 8513-8517• Publication Date (Web): 21 April 2009

Downloaded from http://pubs.acs.org on May 8, 2009

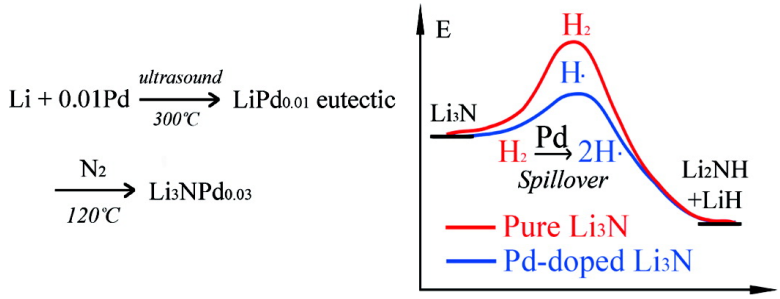

More About This Article

Additional resources and features associated with this article are available within the HTML version:

- Supporting Information
- Access to high resolution figures
- Links to articles and content related to this article
- Copyright permission to reproduce figures and/or text from this article

View the Full Text HTML

ACS Publications
High quality. High impact.

The Journal of Physical Chemistry C is published by the American Chemical Society. 1155 Sixteenth Street N.W., Washington, DC 20036

Hydrogen Spillover Enhanced Hydriding Kinetics of Palladium-Doped Lithium Nitride to Lithium Imide

Chikai Lin, Tao Xu,* Jiamei Yu, Qingfeng Ge, and Zhili Xiao

Department of Chemistry and Biochemistry, Northern Illinois University, Dekalb, Illinois 60115, Department of Chemistry and Biochemistry, Southern Illinois University, Carbondale, Illinois 62901, and Department of Physics, Northern Illinois University, Dekalb, Illinois 60115

Received: February 20, 2009; Revised Manuscript Received: March 30, 2009

Hydrogen storage in complex metal hydrides often suffers from unsatisfied hydriding kinetics of the corresponding complex metals under moderated conditions, partly due to the kinetic barrier associated with the breaking of the H−H bond. Therefore, doping catalysts for H−H bond breakage become a feasible strategy to improve the hydriding kinetics because hydrogen adatoms can efficiently spill over from catalyst to complex metals. To realize this strategy, we developed a unique method to uniformly dope catalytic metal in the storage complex metals via synthesis of the eutectic of the catalytic metal and the precursory storage metal. This method eliminates the use of support materials for catalysts, while still maintaining the large surface area and uniformity of the catalysts. We demonstrated that $Li_3NPd_{0.03}$ with nanoscopic Pd uniformity can be prepared through nitridization of $LiPd_{0.01}$ eutectic. The resulting $Li_3NPd_{0.03}$ exhibits enhanced hydriding kinetics over pure Li_3N for the reaction $Li_3N + H_2 \leftrightarrow Li_2NH + LiH$ under moderate conditions. The activation barrier for the hydriding of $Li_3NPd_{0.03}$ was measured to be ∼28 kJ/mol. DFT calculation reveals that the hydrogen adatom migration barrier from the palladium to the nitrogen atom is ∼25 kJ/mol. These results indicate that the Pd-doped LiN_3 is hydrided by hydrogen adatoms that migrate from the Pd catalyst and the kinetic barrier for such a hydriding process is mainly ascribed to the diffusion barrier of the H adatom from the palladium to the nitrogen atom.

Introduction

Problems related to fossil fuels provide a strong motive to search for alternative energy carriers. Hydrogen emerges as a strong candidate mainly for its abundance and nonpolluting nature. However, the use of hydrogen as an on-board fuel is hindered by the lack of effective hydrogen storage technology.[1] Solid-state hydrogen storage materials are considered as a type of safe and effective hydrogen carrier for transportation application. In general, solids for hydrogen storage include complex metal hydrides and adsorbents with large surface area.[2]

Due to their inherent stoichiometry, many complex metal hydrides can achieve high gravimetric hydrogen concentration. Unfortunately, they often suffer from the elevated temperatures required for overcoming the kinetic and/or thermodynamic barriers during hydriding and dehydriding processes.[3] Considerable efforts have been devoted to destabilizing the complex metals through addition of dopants that reduce the enthalpy gap between the reactants, i.e., complex metals, and the products, i.e., the corresponding hydrides.[3−5] However, less attention was paid to another reaction participant, namely, the H_2 molecule.

The significance of modifying the H_2 molecule has been demonstrated in hydrogen adsorption on solids of large surface area. Yang and co-workers showed that the hydrogen uptake in metal−organic frameworks under moderate condition can be enhanced greatly through hydrogen spillover.[6,7] The concept of hydrogen spillover originated from metal-catalyzed hydrogenation reactions, in which catalytic metal nanoclusters such as Pd or Pt are spread on solid supports with high surface area, e.g., activated carbon, nanoporous alumina, etc.[8] When a dihydrogen molecule is adsorbed on the metal part of the supported catalysts, it dissociates into hydrogen adatoms spontaneously. Some of the H adatoms remain attached to the metal, while others diffuse to the adjacent supports. The process is thus termed hydrogen spillover. The adjacent supports are considered the primary receptors for the spilt hydrogen adatoms. Spillover to a secondary material also occurs and is referred to as secondary spillover.[8] Direct evidence for hydrogen spillover has been observed by inelastic neutron scattering spectroscopy.[9] In comparison to a H_2 molecule, the spillover hydrogen adatoms possess higher diffusivity and activity.[10,11]

Hydrogen storage in complex metal hydrides may also take the advantage of hydrogen spillover. Theoretical work suggests that hydrogen spillover on Pd-doped Mg can reduced the hydriding kinetic barrier of Mg.[12] We thus aim to ease the H−H bond cleavage through direct doping of catalysts in the hosting complex metals. In such hybrid materials, the spillover of atomic hydrogen from catalytic metal sites to the hosting complex metal sites can lead to a kinetically more favorable route for hydriding.

Generally, in order to reach a microscopic uniformity in the prepared materials, a supported catalyst is ball-milled together with the storage materials.[11] However, the use of supported catalysts will increase the intrinsic weight of the storage materials, thereby reducing the hydrogen capacity. In the present work, we report a unique doping method to avoid the use of supports but still maintain the uniformity of the catalyst in the storage material. Our strategy is first to synthesize the eutectic of pure catalytic metal and the storage metals. This is followed by reactions that convert the resulting eutectic to the catalyst-doped complex metal. We choose to dope Li_3N with Pd to exemplify this strategy because either Pd or Pt is a well-studied

* To whom correspondence should be addressed to the Department of Chemistry and Biochemistry, Northern Illinois University. E-mail: txu@niu.edu.

10.1021/jp901598b CCC: $40.75 © 2009 American Chemical Society
Published on Web 04/21/2009

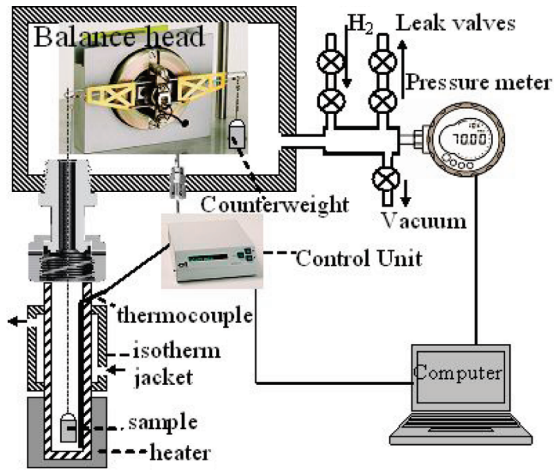

Figure 1. Schematic diagram of the gravimetric measurement unit.

catalyst for hydrogen spillover[9,13] and can form eutectics with lithium at relatively low temperature.[14,15]

Experimental Methods

1. Synthesis. The synthesis of the Li−Pd eutectic was conducted in an argon-filled glovebox (oxygen level <0.3 ppm). First, 0.3 g of lithium (99.9%, Alfa-Aesar) was placed in a nickel crucible that was then heated at 250 °C in a dry block temperature calibrator (Ucal 400+). The selection of Ni crucible is due to its high resistance to lithium below 1000 °C.[16] As the solid lithium liquefies, 0.045 g of Pd grains (99.999%, Alfa-Aesar) was added to the liquid. The mixture with stoichiometry of $LiPd_{0.01}$ was heated at 300 °C for 24 h, during which the liquid maintains a mirror-like surface. To ensure the uniformity of the Pd in lithium, the liquid was further ultrasonicated with a homogenizer equipped with a titanium tip (Sonozap). The hot liquid was quenched by quickly pouring it onto a clean 316 stainless steel plate to avoid segregation of the two components. The solid $LiPd_{0.01}$ was cut into thin pieces and nitridized in ultrapure N_2 (99.999%) at 120 °C (well below its melting point) overnight, similar to the reported synthesis for pure Li_3N.[17] The resulting $Li_3NPd_{0.03}$ (Pd ~10 wt %) is a dark red solid, which was ground into fine powders with a mortar and pestle.

2. Gravimetric Measurement. The gravimetric unit, as illustrated in Figure 1, was home-assembled to perform the gravimetric sorption studies. The core of the gravimetric sorption analyzer is a highly sensitive electromagnetic beam microbalance (C.I Electronics, UK) that can be operated in pressure up to 100 bar. The balance head (Model MK2) is enclosed in a nonmagnetic steel chamber and connected to a high-pressure 8-wire NPT feedthrough (Conax Technology Inc. NY), through which the balance head is interfaced to a control unit for input/output to a computer. The ultimate weight readability can reach 0.1 μg. The sample is placed in a brass cup (weight = 416 mg) hung on one side of the beam, while the counterweight is hung on the other side of the beam. The electric adjustable range of the balance head is 500 mg. With a VCR fitting (Swagelok) at the hang-down port, the sample side is sheathed in a nonmagnetic steel tube for convenient sample loading. In addition, an isothermal jacket is welded to the middle section of the steel tube for flow of coolant, thus a steady temperature distribution along the testing tube can be established, and the region above the cooling jacket is maintained at room temperature. We keep the weight of each sample precisely at 150 mg. After sample loading, the system is vacuumed (<1 mbar), followed by addition of 50 bar of ultrapure hydrogen (99.999%). Prior to heating, the balance is rezeroed at 21 °C and the weight change is recorded at this moment. Next, the lower end of the tube where the sample resides is heated quickly to the desired temperature. The recorded weight change reflects the sum of absorbed hydrogen and any change in buoyancy force after the balance is zeroed. Thus, the actual weight increase due to the absorbed hydrogen can be calibrated by eq 1.

$$W_H = W_r + W_b \quad (1)$$

where W_H is the weight increase due to adsorbed hydrogen, W_r is the weight change recorded by the balance, and W_b is the change of buoyancy force due to the redistribution of gas density upon heating. W_b can also be experimentally obtained by repeating the real experimental condition on a nonsorptive dummy sample, e.g., quartz, which has the same volume as that of 150 mg of Li_3N (0.118 cm^3). The measured W_b is less than 0.08 wt % of the dummy sample weight under the same conditions for real experiments.

On the other hand, the majority of the volume that is affected by buoyancy change resulting from heating is in the sample zone, while temperature gradient in the zone above the isothermal jacket is negligibly small. Therefore, W_b can be estimated as

$$W_b = (V_s + V_c)(\rho_2 - \rho_1) \quad (2)$$

where $V_s = 0.118$ cm^3 is the volume of 150 mg of Li_3N, $V_c = 0.0495$ cm^3 is the volume of the brass container (419 mg), and ρ_1 and ρ_2 are the H_2 density before and after the redistribution of the H_2 density due to heating, which is available from the NIST database (http://webbook.nist.gov/chemistry/fluid/). For example, in 50 bar of H_2, the change in buoyancy force between 20 and 70 °C is only −96.3 μg, corresponding to 0.06 wt % of the sample weight, in accordance with the experimental buoyancy force correction.

3. Characterization. Because all samples are sensitive to air and moisture, they were stored in an argon-filled vial for transportation prior to sample loading into the instrument.

Morphology and compositional study were performed with a Hitachi S-4700-II field emission scanning electron microscope (SEM).

Samples were also investigated on a Hitachi H-600 transmission electron microscope (TEM). The powders were collected by copper grids in the argon glovebox.

Vibrational data were obtained by using an attenuated total reflection Fourier transfer infrared (ATR/FT-IR) spectrometer (ATI Mattson Genesis Series) having a resolution of 4 cm^{-1}. A horizontal solid powder holder, consisting of a ZnSe crystal, was incorporated into the sample compartment to analyze the hydrided $Li_3NPd_{0.03}$ powder. The powder was spread onto the ZnSe surface inside the Ar glovebox and sealed prior to scans.

4. Computational Method. All the calculations were carried out by using the Vienna ab initio silulation package (VASP) code,[18] a density function theory (DFT) program package with plane wave as the basis set. The interaction between ions and electrons was described by using the projector augmented wave method.[19] The plane wave basis set with a cutoff energy of 400 eV was used to expand the wave function of valence electrons. The nonlocal exchange-correlation energy was evaluated by the PBE functional.[20] A (4 × 4 × 1) *k*-point grid was used to sample the surface Brillouin zone of the $Li_3N(100)$ surface slab used in the simulation. The structural optimization was considered converged when the forces on the unconstrained atoms were less than 0.03 eV/Å. A similar method and parameters have been applied to other complex metal hydrides.[21]

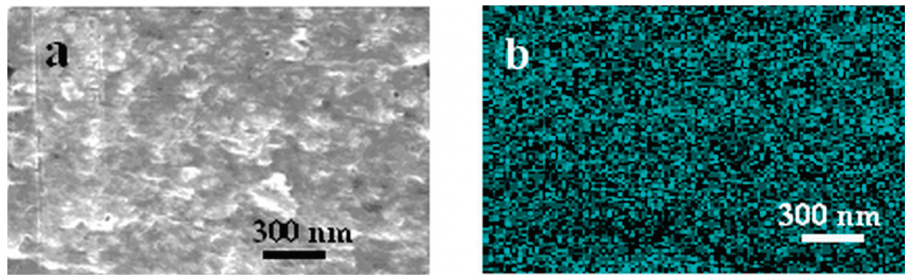

Figure 2. (a) SEM image of the surface of a freshly cut $Li_3Pd_{0.03}$ eutectic; (b) the SEM-EDX Pd mapping image of the same area in panel a.

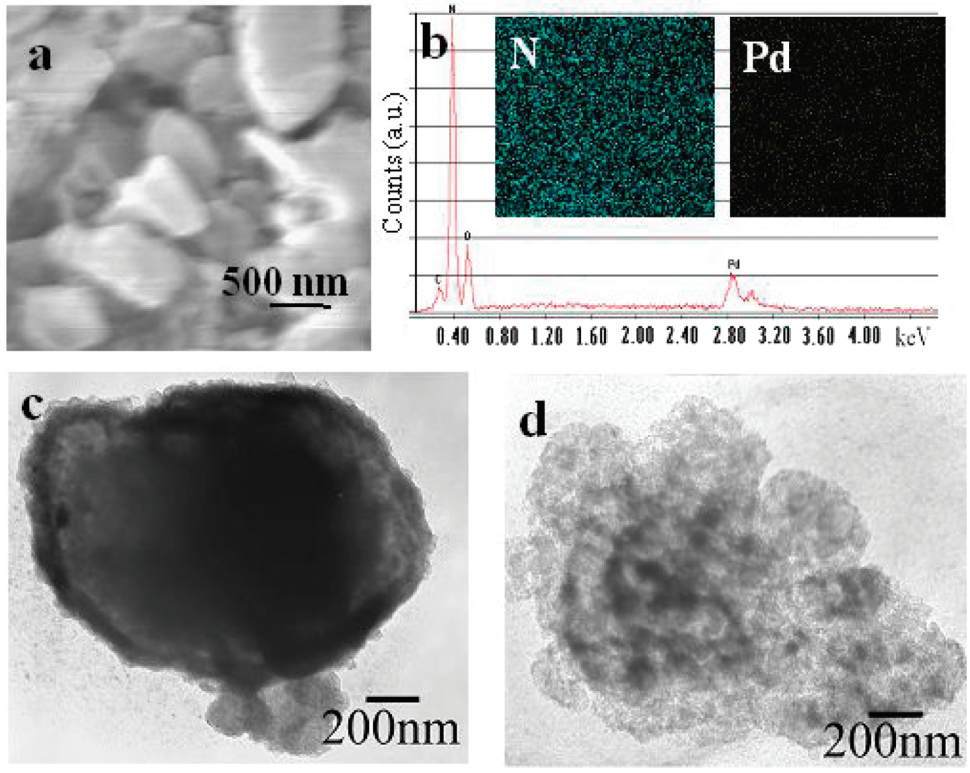

Figure 3. (a) SEM image of $Li_3NPd_{0.03}$ powders; (b) EDX spectrum of the elementary analysis of $Li_3NPd_{0.03}$ powders (inset: SEM-EDX mapping images for N (left) and Pd (right) of the same area in panel a); (c) TEM images of a $Li_3NPd_{0.03}$ particle; and (d) TEM images of a pure Li_3N particle.

Result and Discussion

The phase diagram of the Pd_x−Li system suggests that eutectic of the two metals can form at temperatures below 200 °C when x is less than 0.1.[14] Higher Pd concentration would require higher temperatures, but the experiment at high temperatures can suffer from various problems, including the severe etching of the container by Li and the oxidation of Li with a trace of oxygen. Furthermore, to achieve relatively high gravimetric hydrogen concentration, the weight of storage materials excluding hydrogen content should be kept light. Consequently, we chose $x = 0.01$ since the corresponding Pd weight concentration already reaches 10 wt % in the $Li_3NPd_{0.03}$ product. Figure 2 presents the survey SEM image taken from a freshly cut surface of a $LiPd_{0.01}$ eutectic specimen and the corresponding nanoscopic Pd distribution map acquired by an energy-dispersive X-ray (EDX) detector. Pd was observed in a uniform distribution throughout the films examined. Li was not detectable because its atomic number is less than 5.

To avoid resegregation of Pd in the eutectic, the nitridization of $Li_3NPd_{0.03}$ was carried out through a solid−gas reaction by keeping the temperature below the melting point of lithium. Figure 3a is a survey SEM image of the $Li_3NPd_{0.03}$ powders. The EDX element spectrum (Figure 3b) confirmed the existence of N and Pd. The EDX composition analysis revealed that the atomic ratio of N to Pd is ca. 99.7:3, in according with the stoichiometry of $Li_3NPd_{0.03}$. The presence of oxygen and carbon in EDX is inevitable since the sample was loaded in air. The corresponding EDX mapping images for Pd and N are shown in the insets of Figure 3b. It is clear that even at nanometer scale, Pd is distributed as uniformly as nitrogen. Figure 3c shows a TEM image of the $Li_3NPd_{0.03}$ powders and pure Li_3N powder (Figure 3d) as comparison. Under identical electron beam energy (75 keV) and similar powder size and thickness, the TEM image of $Li_3NPd_{0.03}$ appears much darker than that of pure Li_3N. This can be ascribed to the greater atomic number of Pd than that of Li and N.[22] The TEM images also support that Pd is uniformly distributed in the Li_3N.

The hydriding of $Li_3NPd_{0.03}$ was conducted in 50 bar of H_2. Figure 4 exhibits the gravimetric analysis of the calibrated increased weight percentage versus time profiles at 21, 39, 50, and 70 °C, respectively. For comparison, the hydriding of pure Li_3N was also measured at 21, 50, and 70 °C, respectively. In comparison to pure Li_3N, Pd-doped Li_3N exhibits a markedly enhanced hydriding rate, by a factor of 2−3 at temperatures of

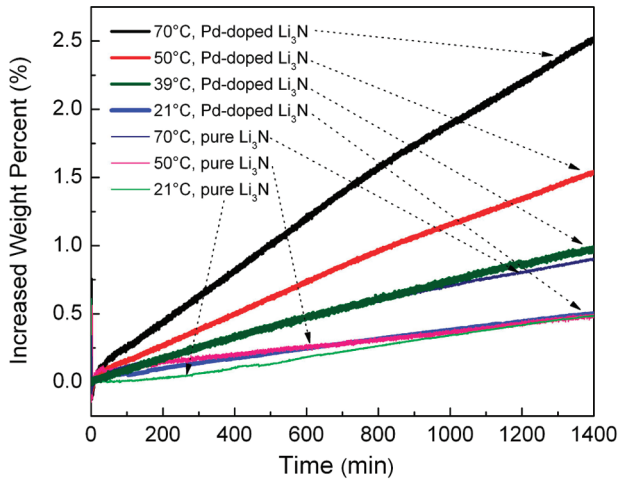

Figure 4. Kinetic hydriding curves for pure Li_3N and $Li_3NPd_{0.03}$ measured by gravimetric sorption analyzer.

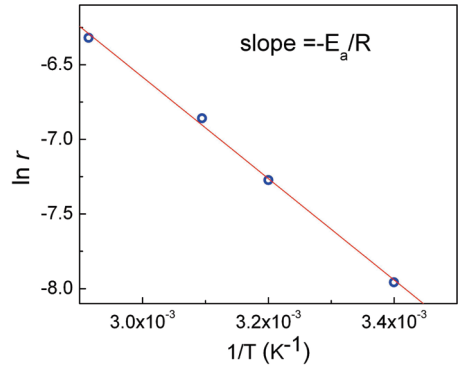

Figure 5. Plot of ln r versus $1/T$. The red line is the linear fit. The slope is -3397 ± 180 mol·K, which corresponds to $E_a = 28 \pm 2$ kJ/mol.

50 and 70 °C. Although Pd also adsorbs hydrogen, the maximum contribution from Pd is less than 0.1%, considering the relatively low H_2 uptake of Pd (~1.0 wt % at 50 bar[23]) and the small amount of Pd in the mixture (10 wt %). Therefore, Pd played the role of catalyst for hydrogen dissociation and spillover but contributed little to the hydrogen storage capacity. The hydriding of $Li_3NPd_{0.03}$ appears to be a zeroth order reaction. Thus the reaction rate can be determined by measuring the slopes of the hydriding curves, yielding 1.8×10^{-3}, 1.1×10^{-3}, 6.9×10^{-4}, and 3.5×10^{-4} wt % min^{-1} for 70, 50, 39, and 21 °C, respectively. Furthermore, for a zeroth order reaction, the reaction rate r equals the rate constant k, so one can use the Arrhenius equation (eq 3) to estimate the kinetic barrier for the hydriding of $Li_3NPd_{0.03}$.

$$\ln r = \ln k = \ln A - \frac{E_a}{R}\left(\frac{1}{T}\right) \quad (3)$$

where A is the prefactor, E_a is the activation energy, R is the ideal gas constant, and T is temperature. From the plot of ln r versus $1/T$ shown in Figure 5, we obtained an activation barrier, E_a, of ~28 ± 2 kJ/mol. Dissociative adsorption of hydrogen over Pd surfaces has been shown as a barrierless process whereas dissociation requires two or more vacancy sites to accommodate the H adatoms.[24,25] The zeroth nature of the hydrogenation kinetics indicated that the process is not limited by hydrogen dissociation but by the diffusion of hydrogen adatoms.

We used a Pd_4 cluster that resides on the (100) surface of Li_3N to analyze the hydrogen adsorption and migration processes

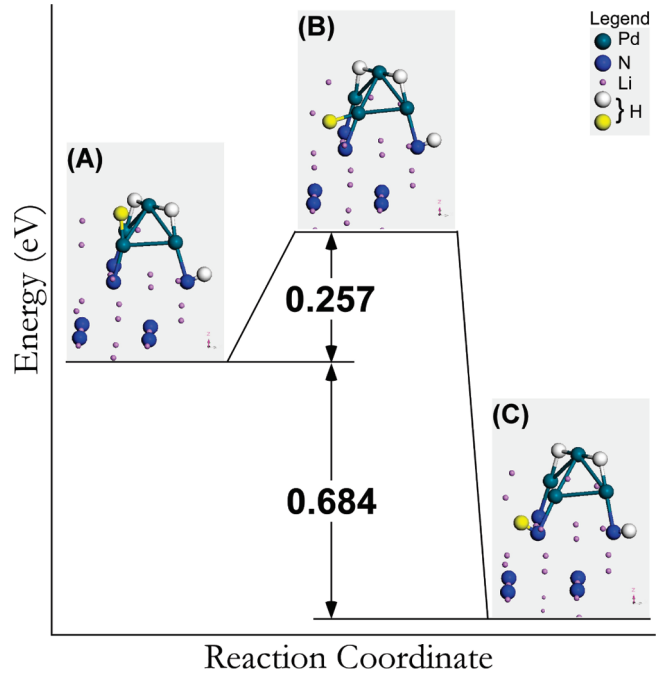

Figure 6. Potential energy profile of H adatom diffusion from Pd to N. The bright blue balls represent N atoms, the small pink balls are Li atoms and the interconnected greenish blue balls represent a Pd_4 cluster, the yellow ball represents a diffusing H adatom from Pd_4 to N atom, and the white balls are stationary H atoms that are bound to a Pd atom or a N atom. Inset A shows an H adatom that starts to migrate from the bridge-bound configuration on the Pd_4 cluster to the N atom in the Li_3N slab. Inset B is a transition state. Inset C shows the H atoms that are finally bound to the N atom, forming an N−H bond.

and determined the diffusion barrier using the DFT calculations. There are numerous configurations that may be formed from the H adatoms and the supported Pd_4 and/or N atoms of Li_3N. In the present study, we selected the (100) surface of Li_3N as it has the lowest surface energy among the low index surfaces. The surface was modeled by a supercell with a dimension of 7.23 Å × 7.76 Å × 23.49 Å. Sixteen Li_3N molecular units were distributed in a 7-layer slab. The bottom five layers were frozen in their bulk positions, whereas the remaining layers together with the Pd_4 cluster and adsorbed hydrogen atoms were allowed to relax. Herein, we focus on the migration of the hydrogen adatom from the Pd_4 to the neighboring N site. Figure 6 shows a potential energy profile for a hydrogen adatom to diffuse from the bridge-bound configuration on the Pd_4 cluster (inset A in Figure 6) to the nearby N atom in the Li_3N slab (inset C in Figure 6). As shown in Figure 6, the overall process for H from the state of being adsorbed on the Pd_4 cluster to the state of being bound to N is energetically favorable, manifested by an energy gain of 0.684 eV. This diffusion process is activated through a transition state (inset B in Figure 6). The activation barrier for this diffusion step is calculated to be 0.257 eV (~25 kJ/mol). This result is in good agreement with the value from analysis of the experimental kinetic data. Thus, we believe the kinetic barrier obtained from the experiments is mainly attributed to the diffusion barrier of H adatom from palladium to nitrogen atom, namely the energy barrier for H adatom spillover from Pd to the N atom in Li_3N. The hydriding of Pd-doped Li_3N is the result of the reaction between Li_3N and the spillover H adatom and the rate-limiting step in hydriding of Pd-doped Li_3N is the translocation of the H adatom from Pd sites to N sites.

It is known that the hydriding process for pure Li_3N undergoes a two-step reaction: (1) $Li_3N + H_2 \leftrightarrow Li_2NH + LiH$ and (2)

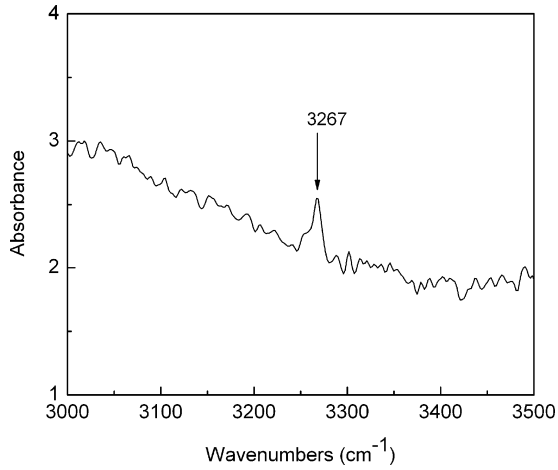

Figure 7. ATR/FT-IR spectrum of hydrogenated $Li_3NPd_{0.03}$ at 70 °C.

$Li_2NH + H_2 \leftrightarrow LiNH_2 + LiH$.[17,26] Reaction 1 starts to occur when the temperature is higher than 70 °C, while reaction 2 requires temperature above 250 °C. The hydrogen weight percentage increases for 5.8% in eqs 1 and 2 with respect to Li_3N. The product of the hydrided Pd-doped Li_3N was analyzed by ATR/FT-IR, as shown in Figure 7. If the product contains lithium amide $LiNH_2$, one would expect two peaks at 3312 and 3259 cm^{-1}, corresponding to asymmetric and symmetric stretching of N−H bonds in $LiNH_2$ molecules.[27−29] However, the IR spectrum shows only one peak at 3267 cm^{-1}, which agrees with the N−H stretching mode in lithium imide Li_2NH.[27] Therefore, infrared study suggests that only reaction 1 occurred for Pd-doped Li_3N under 70 °C. The formation of Li_2NH was also confirmed by our computational frequency analysis for isolated Li_2NH molecule and the corresponding bulk system. Our results show that the N−H stretch mode of the Li_2NH molecule is at 3355 cm^{-1}. The same mode spans the range of 3261−3277 cm^{-1} in bulk Li_2NH.

Conclusions

In summary, the concept of improving hydriding kinetics of complex metals through hydrogen spillover is demonstrated in Pd-doped Li_3N. Different from conventional ball milling, the doping of Pd catalyst in lithium nitride was achieved through the nitridization of $LiPd_{0.01}$ eutectic. This method provided an alternative doping strategy that eliminates the use of support materials. As Pd plays the role of catalyst to dissociate H_2, with the produced hydrogen adatoms to spill over from Pd to Li_3N, the resulting $Li_3NPd_{0.03}$ exhibits faster hydriding rate over pure Li_3N in the reaction of $Li_3N + H_2 \leftrightarrow Li_2NH + LiH$. The kinetic barrier for the reaction was measured to be ∼28 kJ/mol, which is in agreement with the calculated barrier for the diffusion of hydrogen adatoms from Pd_4 to the N atom in Li_3N. These results indicate that the Pd-doped LiN_3 is hydrided by hydrogen adatoms that migrate from the Pd catalyst, and the kinetic barrier for such a hydriding process is mainly ascribed to the diffusion barrier of the H adatom from the palladium to the nitrogen atom. Our current work suggests that catalytic metals doped in hydrogen storing complex metals can ease the H−H bond cleavage, and the spillover of the resulting H adatoms can lead to the hydriding of complex metals via a kinetically more favorable pathway.

Acknowledgment. This work was supported by the American Chemical Society Petroleum Research Fund (Type G 46374-G10). J.Y. and Q.G. acknowledge the support of US-DOE (Contract no. DE-FG02-05ER46231). We also acknowledge the technical support from Ms. Lori Bross and Mr. Larry Gregersen.

References and Notes

(1) Crabtree, G. W.; Dresselhaus, M. S.; Buchanan, M. V. *Phys. Today* **2004**, *57*, 39–45.
(2) Schlapbach, L.; Züttel, A. *Nature (London)* **2001**, *414*, 353–358.
(3) Orimo, S.; Nakamori, Y.; Eliseo, J. R.; Züttel, A.; Jensen, C. M. *Chem. Rev.* **2007**, *107*, 4111–4132.
(4) Liu, J.; Ge, Q. *J. Phys. Chem. B* **2006**, *110*, 25863–25868.
(5) Lu, J.; Fang, Z. Z.; Sohn, H. Y.; Bowman, R. C., Jr.; Hwang, S. J. *J. Phys. Chem. C* **2007**, *111*, 16686–16692.
(6) Li, Y.; Yang, R. T. *J. Am. Chem. Soc.* **2006**, *128*, 726–727.
(7) Li, Y.; Yang, R. T. *J. Am. Chem. Soc.* **2006**, *128*, 8136–8137.
(8) Conner, W. C., Jr.; Falconer, J. L. *Chem. Rev.* **1995**, *95*, 759–788.
(9) Mitchell, P. C. H.; Ramirez-Cuesta, A. J.; Parker, S. F.; Tomkinson, J.; Thompsett, D. *J. Phys. Chem. B* **2003**, *107*, 6838–6845.
(10) Rowsell, J. L. C.; Yaghi, O. M. *Angew. Chem., Int. Ed.* **2005**, *44*, 4670–4679.
(11) Wang, L.; Yang, R. *Energy Environ. Sci.* **2008**, *1*, 268–279.
(12) Du, A. J.; Smith, S. C.; Yao, X. D.; Lu, G. Q. *J. Am. Chem. Soc.* **2007**, *129*, 10201–10204.
(13) Back, C.; Sandi, G.; Prakash, J.; Hranisavljevic, J. *J. Phys. Chem. B* **2006**, *110*, 16225–16231.
(14) Sangster, J.; Pelton, A. D. *J. Phase Equilib.* **1992**, *13*, 63–65.
(15) Okamoto, H. *J. Phase Equilib. Diffus.* **1993**, *14*, 653–654.
(16) Lee, K. J.; Lee, S. Y.; Nash, P. In *Binary Alloy Phase Diagrams*, 2nd ed.; Massalski T. B., Editor-in-chief; Materials Information Soc.: Materials Park, OH, 1990; Vol. 3.
(17) Chen, P.; Xiong, Z.; Luo, J.; Liu, J.; Tan, L. K. *Nature (London)* **2002**, *420*, 302–304.
(18) Kresse, G.; Furthmuller, J. *VASP Guide*, 2007, http://cms.mpi.univie.ac.at/vasp.
(19) Kresse, G.; Joubert, D. *Phys. Rev. B* **1999**, *59*, 1758.
(20) Perdew, J. P.; Burke, K.; Ernzerhof, M. *Phys. Rev. Lett.* **1996**, *77*, 3865.
(21) (a) Ge, Q. *J. Phys. Chem. A* **2004**, *108*, 8682. (b) Liu, J.; Han, Y.; Ge, Q. *Chem.—Eur. J.* **2009**, *15*, 1685.
(22) Reimer, L. *Transmission Electron Microscopy−Physics of Image Formation and Microanalysis*, 3rd ed.; Springer-Verlag: Berlin, Germany, 1993; Chapter *5*, pp 136−168.
(23) Sakamoto, Y.; Takai, K.; Takashima, I.; Imada, M. *J. Phys.: Condens. Matter* **1996**, *8*, 3399–3411.
(24) Mitsui, T.; Rose, M. K.; Fomin, E.; Ogletree, D. F.; Salmeron, M. *Nature (London)* **2003**, *422*, 705–707.
(25) Gross, A.; Dianat, A. *Phys. Rev. Lett.* **2007**, *98*, 206107.
(26) Hu, Y. H.; Ruckenstein, E. *Ind. Eng. Chem. Res.* **2006**, *45*, 4993–4998.
(27) Bohger, J. P. O.; Essmann, R. R.; Jacobs, H. *J. Mol. Struct.* **1995**, *348*, 325–328.
(28) Chen, P.; Xiong, Z.; Luo, J.; Lin, J.; Tan, L. *J. Phys. Chem. B* **2003**, *107*, 10967–10970.
(29) Kojima, Y.; Kawai, Y. *J. Alloys Compd.* **2005**, *395*, 236–239.

JP901598B